ECCOMAS Congress 2016
VII European Congress on Computational Methods in Applied Sciences and Engineering
M. Papadrakakis, V. Papadopoulos, G. Stefanou, V. Plevris (eds.)
Crete Island, Greece, 5–10 June 2016

NUMERICAL VALIDATION OF A FOUR PARAMETER LOGARITHMIC TURBULENCE MODEL

D. Cerroni[1], R. Da Vià[1*], S. Manservisi[1] and F. Menghini[1]

[1] DIN - Lab. of Montecuccolino, University of Bologna, Via dei Colli 16, 40136 Bologna, Italy
[*] e-mail: roberto.davia2@unibo.it

Keywords: Turbulent heat transfer, Turbulence modeling

Abstract. *Computational Fluid Dynamics codes are used in many industrial applications in order to evaluate interesting physical quantities, such as the heat transfer in turbulent flows. Commercial CFD codes use only turbulence models with an imposed constant turbulent Prandtl number Pr_t, which can give accurate results only for simulations when a strong similarity between the velocity field and the temperature field can be assumed. For fluids with a low Prandtl number, as for heavy liquid metals, a constant turbulent Prandtl number leads to an overestimation of the heat transfer, so experimental results and Direct Numerical Simulation cannot be reproduced. In this work we propose a new k-Ω-k_θ-Ω_θ turbulence model as an improvement of the k-ω-k_θ-ω_θ turbulence model, already validated by the authors, where Ω and Ω_θ are calculated as the natural logarithm of the variables ω and ω_θ. With this reformulation of the previous turbulence model we obtain some important advantages in numerical stability and robustness of the code. Results for the simulations of fully developed turbulent flows in two and three dimensional geometries are reported and compared with experimental correlations and DNS data, when available.*

1 Introduction

The IV generation of nuclear reactors is based on a design that combines increased safety, passive safety systems and low radioactive-waste production. Six new reactors have been proposed by Generation IV International Forum (GIF). Among them the Lead Fast Reactor and the Sodium Fast Reactor are cooled by a liquid metal. One of the main features of these reactors is the capability to produce fissile atoms by the transmutation of Uranium-238. In order to obtain this, a material with high atomic mass, such as liquid metals, has to be employed as core-coolant. Inside a nuclear reactor core the fluid flow is typically turbulent so a turbulence model is needed to simulate the flow with affordable computational cost.

The most common turbulence models currently employed for the study of turbulent flows are based on the Reynolds Average of the Navier Stokes equations (RANS models). In these models the similarity between the velocity and the thermal turbulent fields is usually assumed. An algebraic relation based on the eddy viscosity and the turbulent Prandtl number is used to compute the turbulent heat flux. This turbulence model is known as Simple Eddy Diffusivity (SED) model. In the SED model one computes the eddy viscosity ν_t by using two turbulent variables, such as the turbulent kinetic energy k and its dissipation rate ε. The eddy thermal diffusivity α_t is then computed as $\alpha_t = \nu_t/Pr_t$. This procedure can be used when turbulent flows with a molecular Prandtl number $Pr \simeq 1$ are simulated. Heavy liquid metals such as mercury, Lead-Bismuth Eutectic (LBE) and sodium-potassium alloys are characterized by a low molecular Prandtl number, varying from 0.01 to 0.05. In these fluids heat conduction is an important heat transfer mechanism and the similarity assumption between the velocity and the temperature fields does not hold. It is well known that when the standard SED model is adopted with low Prandtl numbers the obtained values of heat transfer are very different from the experimental ones. This problem can be solved by specifying the Pr_t for each geometry or using a more sophisticated turbulence model in order to define the proper thermal characteristics time scales [1, 2, 3, 4, 5].

In this paper we present a new logarithmic formulation of the four parameter k-ω-k_θ-ω_θ turbulence model for liquid metal flows. We briefly recall the RANS equations and the first formulation of a four parameter k-ε-k_θ-ε_θ, then we derive the k-ω formulation already validated by the authors [6, 7, 8, 9]. Finally the new logarithmic k-Ω-k_θ-Ω_θ model is presented. A discussion on the boundary conditions is reported to better motivate the derivation of this model. We report some numerical results obtained with the implementation of the logarithmic model in a finite element in-house code and compare them with experimental correlations and DNS data, when available.

2 Transport equations and turbulence models

Inside the nuclear reactor core the flow of liquid metal can be considered incompressible so the system of equations to be solved is based on the Reynolds Averaged incompressible Navier Stokes equations, namely

$$\boldsymbol{\nabla}\cdot\mathbf{u} = 0\,, \tag{1}$$

$$\rho\frac{\partial\mathbf{u}}{\partial t}+\rho(\mathbf{u}\cdot\boldsymbol{\nabla})\mathbf{u} = \boldsymbol{\nabla}\cdot\boldsymbol{\sigma}-\boldsymbol{\nabla}\cdot\boldsymbol{\tau}^R+\rho\mathbf{g}\,, \tag{2}$$

$$\rho C_p\left(\frac{\partial T}{\partial t}+(\mathbf{u}\cdot\boldsymbol{\nabla})T\right) = \boldsymbol{\nabla}\cdot\mathbf{q}-\boldsymbol{\nabla}\cdot\mathbf{q}^R+Q\,, \tag{3}$$

where $\mathbf{u}$ is the averaged velocity of the fluid and T is the averaged temperature. The tensors $\boldsymbol{\sigma}$ and $\mathbf{q}$ are the usual viscous stress and heat flux and they are modeled using Navier-Stokes constitutive law for viscous fluids and Fourier law for heat conduction

$$\boldsymbol{\sigma} := -p\mathbf{I} + \mu\mathbf{D} \quad \text{with} \quad \mathbf{D} := \boldsymbol{\nabla}\mathbf{u} + \boldsymbol{\nabla}\mathbf{u}^T \tag{4}$$

$$\mathbf{q} := -\lambda\boldsymbol{\nabla}T\,. \tag{5}$$

The transport equations for the averaged velocity and temperature are similar to the ones for the instantaneous quantities, except for the terms $\boldsymbol{\tau}^R$ and $\mathbf{q}^R$ which are introduced, as a result of the average procedure over time, in the following form

$$\boldsymbol{\tau}^R = \rho\overline{\mathbf{u}'\mathbf{u}'} \qquad \mathbf{q}^R = \rho C_p\overline{\mathbf{u}'T'}\,, \tag{6}$$

where the operator $\overline{(\cdot)}$ means the time average. These terms are known as the Reynolds stresses and the turbulent heat flux. They could be computed by solving the appropriate transport equations, which means a total number of 9 additional unknowns. This procedure is very expensive in terms of computational cost. Instead of solving these additional transport equations we approximate the terms $\overline{\mathbf{u}'\mathbf{u}'}$ and $\overline{\mathbf{u}'T'}$ by using the eddy diffusivities and the gradients of mean velocity and temperature in the following form

$$\boldsymbol{\tau}^R = -\nu_t\left(\boldsymbol{\nabla}\mathbf{u} + \boldsymbol{\nabla}\mathbf{u}^T\right) + \frac{2k}{3}\mathbf{I}\,, \tag{7}$$

$$\mathbf{q}^R = -\alpha_t\,\boldsymbol{\nabla}T\,, \tag{8}$$

where the eddy diffusivity of momentum ν_t and the heat eddy diffusivity α_t must be properly defined in the turbulence model. The two eddy diffusivities are calculated as a function of the turbulent kinetic energy and of two characteristic time scales: τ_{lu} for the dynamical and $\tau_{l\theta}$ for the thermal turbulence. These time scales have to be defined appropriately in the turbulence model, for details one can see [3, 4, 5, 7].

2.1 The k-ε-k_θ-ε_θ turbulence model

We can define the turbulent kinetic energy k, its dissipation ε, the temperature fluctuations variance k_θ and its dissipation ε_θ as

$$k = \frac{1}{2}\overline{\mathbf{u}'^2}\,, \qquad \varepsilon = \nu\overline{\|\boldsymbol{\nabla}\mathbf{u}'\|^2}\,, \tag{9}$$

$$k_\theta = \frac{1}{2}\overline{T'^2}\,, \qquad \varepsilon_\theta = \alpha\overline{\|\boldsymbol{\nabla}T'\|^2}\,. \tag{10}$$

The transport equations for the variables in (9) and (10) are obtained by taking appropriate moments of the Navier-Stokes equations for the fluctuating quantities $\mathbf{u}'$ and T'. The equation for k is

$$\frac{\partial k}{\partial t} + (\mathbf{u}\cdot\boldsymbol{\nabla})k = \boldsymbol{\nabla}\cdot\left[\left(\nu + \frac{\nu_t}{\sigma_k}\right)\boldsymbol{\nabla}k\right] + P_k - \varepsilon\,, \tag{11}$$

where

$$P_k := -\overline{u_i'u_j'}\,\frac{\partial u_i}{\partial x_j} = \frac{\nu_t}{2}\|\boldsymbol{\nabla}\mathbf{u} + \boldsymbol{\nabla}\mathbf{u}^T\|^2\,, \tag{12}$$

is the source term of the transport equation. The equation for ε has this form

$$\frac{\partial \varepsilon}{\partial t} + (\mathbf{u}\cdot\boldsymbol{\nabla})\varepsilon = \boldsymbol{\nabla}\cdot\left[\left(\nu + \frac{\nu_t}{\sigma_\varepsilon}\right)\boldsymbol{\nabla}\varepsilon\right] + C_{1\varepsilon}\,\frac{\varepsilon}{k}P_k - C_{2\varepsilon}\frac{\varepsilon^2}{k}f_\varepsilon\,. \tag{13}$$

$C_{1\varepsilon}$	$C_{2\varepsilon}$	C_μ	σ_k	σ_ε
1.5	1.9	0.09	1.4	1.4

Table 1: Values of the model constants for (11) and (13).

The values of the model constants that appear in (11) and (13) are reported in Table 1, while f_ε is a model function defined as

$$f_\varepsilon = (1 - \exp(-0.3226\, R_\delta))^2 \left(1 - 0.3 \exp(-0.0237\, R_t^2)\right) . \tag{14}$$

By defining the characteristic time $\tau_u = k/\varepsilon$ one can model the local dynamical time τ_{lu} in many ways [7, 8, 9].

For the thermal turbulence the two transport equations are

$$\frac{\partial k_\theta}{\partial t} + (\mathbf{u} \cdot \boldsymbol{\nabla}) k_\theta = \boldsymbol{\nabla} \cdot \left[(\alpha + \frac{\alpha_t}{\sigma_{k_\theta}}) \boldsymbol{\nabla} k_\theta \right] + P_\theta - \varepsilon_\theta \,, \tag{15}$$

where

$$P_\theta := -\overline{\mathbf{u}' T'} \cdot \boldsymbol{\nabla} T = \alpha_t \, \|\boldsymbol{\nabla} T\|^2 \,, \tag{16}$$

is the source term in the k_θ transport equation. The equation for ε_θ can be written as [7, 11]

$$\frac{\partial \varepsilon_\theta}{\partial t} + (\mathbf{u} \cdot \boldsymbol{\nabla}) \varepsilon_\theta = \boldsymbol{\nabla} \cdot \left[(\alpha + \frac{\alpha_t}{\sigma_{\varepsilon_\theta}}) \boldsymbol{\nabla} \varepsilon_\theta \right] + \frac{\varepsilon_\theta}{k_\theta} \left(C_{p1}\, P_\theta - C_{d1}\, \varepsilon_\theta \right) + \frac{\varepsilon_\theta}{k} \left(C_{p2}\, P_k - C_{d2}\, \varepsilon \right) . \tag{17}$$

For heavy liquid metals with $Pr \approx 0.025$ we have used the coefficients defined in [3, 4], namely $C_{d1} = 0.9$, $C_{p2} = 0.9$. The coefficient C_{p1} has been set to 0.925 and

$$C_{d2} = 1.9\,(1 - 0.3\, \exp(-0.0237\, R_t^2))(1 - \exp(-0.0308\, R_\delta))^2 . \tag{18}$$

We define a time scale τ_θ as the ratio between k_θ and ε_θ. For details on the time scales and functions to be used in the definition of the eddy viscosity and diffusivity one can see [5, 7, 8, 9, 10, 11].

2.2 The k-ω-k_θ-ω_θ turbulence model

The results obtained with the k-ε-k_θ-ε_θ turbulence model, in terms of the Nusselt number value for the evaluation of the global heat transfer, are more accurate than the ones obtained with the SED model when compared with the reference correlations for liquid metals [7, 8, 9]. The k-ε model better matches experimental results but shows poor numerical convergence due to the strong coupling of ε-ε_θ with k-k_θ on wall boundaries. In order to avoid this coupling between the state variables we develop a k-ω-k_θ-ω_θ model where ε-ε_θ are replaced by the turbulent kinetic energy specific dissipation ω and the specific dissipation of mean squared temperature fluctuations ω_θ defined as

$$\omega = \frac{\varepsilon}{C_\mu k} \qquad \omega_\theta = \frac{\varepsilon_\theta}{C_\mu k_\theta} \,. \tag{19}$$

$C_{1\varepsilon}$	$C_{2\varepsilon}$	C_μ	σ_k	σ_ε	c_{p1}	c_{p2}	c_{d1}	σ_θ
1.5	1.9	0.09	1.4	1.4	1.025	1.9	1.1	1.4

Table 2: Values of the model constants for (20) - (23).

This new turbulence model is obtained by substituting (19) into (11-13-15-17). This keeps the accuracy of the results and enhances the algorithm stability [6]. The new system of equations is

$$\frac{\partial k}{\partial t} + \mathbf{u}\cdot\boldsymbol{\nabla} k = \boldsymbol{\nabla}\cdot\left[\left(\nu + \frac{\nu_t}{\sigma_k}\right)\nabla k\right] + P_k - C_\mu\, k\,\omega\,, \tag{20}$$

$$\frac{\partial \omega}{\partial t} + \mathbf{u}\cdot\boldsymbol{\nabla}\omega = \boldsymbol{\nabla}\cdot\left[\left(\nu + \frac{\nu_t}{\sigma_\varepsilon}\right)\boldsymbol{\nabla}\omega\right] + \frac{2}{k}\left(\nu + \frac{\nu_t}{\sigma_\varepsilon}\right)\boldsymbol{\nabla} k\cdot\boldsymbol{\nabla}\omega + + (c_{\varepsilon 1} - 1)\,\frac{\omega}{k} P_k - C_\mu\,(c_{\varepsilon 2} f_\varepsilon - 1)\,\omega^2\,, \tag{21}$$

$$\frac{\partial k_\theta}{\partial t} + \mathbf{u}\cdot\boldsymbol{\nabla} k_\theta = \boldsymbol{\nabla}\cdot\left[\left(\alpha + \frac{\alpha_t}{\sigma_\theta}\right)\boldsymbol{\nabla} k_\theta\right] + P_\theta - C_\mu\, k_\theta\,\omega_\theta\,, \tag{22}$$

$$\frac{\partial \omega_\theta}{\partial t} + \mathbf{u}\cdot\boldsymbol{\nabla}\omega_\theta = \boldsymbol{\nabla}\cdot\left[\left(\alpha + \frac{\alpha_t}{\sigma_\theta}\right)\boldsymbol{\nabla}\omega_\theta\right] + \frac{2}{k_\theta}\left(\alpha + \frac{\alpha_t}{\sigma_\theta}\right)\boldsymbol{\nabla} k_\theta\cdot\boldsymbol{\nabla}\omega_\theta + + (c_{p1} - 1)\,\frac{\omega_\theta}{k_\theta} P_\theta + c_{p2}\frac{\omega_\theta}{k} P_k - (c_{d1} - 1)\, C_\mu \omega_\theta^2 - c_{d2} C_\mu \omega\omega_\theta\,. \tag{23}$$

The values of the model constants that appear in the system (20) - (23) are reported in Table 2.

2.2.1 Boundary conditions for the turbulence models

Since we do not use wall functions, the exact boundary conditions that must be imposed on wall boundaries can be obtained using a near wall Taylor series expansion for the turbulence variables. These variables are expanded based on their analytical formulation (9-10) and (19) under the constraints imposed by the velocity components on wall boundaries. For k, ε, k_θ and ε_θ we obtain the following asymptotic expressions

$$k_w = \frac{1}{2}\, a\,\delta^2, \qquad \varepsilon_w = \nu\frac{k_w}{\delta^2} = \frac{1}{2}\nu\, a\,, \tag{24}$$

$$k_{\theta w} = \frac{1}{2}\, a_\theta\,\delta^2, \qquad \varepsilon_{\theta w} = \alpha\frac{k_{\theta w}}{\delta^2} = \frac{1}{2}\alpha\, a_\theta\,. \tag{25}$$

From (24) and (25) we see that ε and ε_θ are constant and their values depend on a and a_θ which are related to the velocity and temperature fluctuations that are not known *a priori*. With the change of variables introduced in the k-ω turbulence model the boundary values for are

$$\omega = \frac{\varepsilon}{C_\mu k} = \frac{2\nu}{C_\mu \delta^2}\,, \qquad \omega_\theta = \frac{\varepsilon_\theta}{C_\mu k_\theta} = \frac{2\alpha}{C_\mu \delta^2}\,, \tag{26}$$

so their values depend only on the physical properties of the fluid (ν and α) and on the wall distance (δ^2). For the new variables ω and ω_θ it is possible to set exact Dirichlet b. c., while for k and k_θ we set the following Neumann b. c.

$$\frac{\partial k}{\partial n} = 2\frac{k}{\delta}\,, \qquad \frac{\partial k_\theta}{\partial n} = 2\frac{k_\theta}{\delta}\,, \tag{27}$$

where n indicates the direction normal to the wall surface. The latter condition in (27) can be applied when temperature fluctuations are assumed to be zero at the wall.

2.3 The logarithmic turbulence model k-Ω-k_θ-Ω_θ

The turbulence model we propose here consists in a further improvement of the previous models. The formulation of this new turbulence model is based on [12] in which the various k-ε, k-ω and k-τ models for dynamic turbulence are analyzed in their formulation with logarithmic variables. The introduction of logarithmic variables brings important advantages to the turbulence model, in particular the fact that the original variables are always kept positive because they are calculated as the exponential values of the new logarithmic variables, so this ensures an increased numerical stability. Another important feature is that the logarithmic variables have profiles that are smoother than the ones of the natural variables [12]. In this new turbulence model we use the logarithmic forms of the specific dissipations ω and ω_θ

$$\Omega = \ln(\omega)\,, \qquad \Omega_\theta = \ln(\omega_\theta)\,. \tag{28}$$

For these new variables we can set exact Dirichlet boundary conditions

$$\Omega_w = \ln(\omega_w) = \ln\left(\frac{2\nu}{C_\mu}\right) - 2\ln(\delta)\,, \tag{29}$$

$$\Omega_{\theta w} = \ln(\omega_{\theta w}) = \ln\left(\frac{2\alpha}{C_\mu}\right) - 2\ln(\delta)\,. \tag{30}$$

The new system of equations is

$$\frac{\partial k}{\partial t} + \mathbf{u}\cdot\boldsymbol{\nabla}k = \boldsymbol{\nabla}\cdot\left[\left(\nu + \frac{\nu_t}{\sigma_k}\right)\boldsymbol{\nabla}k\right] + P_k - C_\mu\, k\, e^{\Omega}\,, \tag{31}$$

$$\begin{aligned}\frac{\partial \Omega}{\partial t} + \mathbf{u}\cdot\boldsymbol{\nabla}\Omega = {}& \boldsymbol{\nabla}\cdot\left[\left(\nu + \frac{\nu_t}{\sigma_\varepsilon}\right)\boldsymbol{\nabla}\Omega\right] + \frac{2}{k}\left(\nu + \frac{\nu_t}{\sigma_\varepsilon}\right)\boldsymbol{\nabla}k\cdot\boldsymbol{\nabla}\Omega + \\ & + \left(\nu + \frac{\nu_t}{\sigma_\varepsilon}\right)\boldsymbol{\nabla}\Omega\cdot\boldsymbol{\nabla}\Omega + \frac{c_{\varepsilon 1}-1}{k}P_k - C_\mu\left(c_{\varepsilon 2} f_{exp} - 1\right)e^{\Omega}\,,\end{aligned} \tag{32}$$

$$\frac{\partial k_\theta}{\partial t} + \mathbf{u}\cdot\boldsymbol{\nabla}k_\theta = \boldsymbol{\nabla}\cdot\left[\left(\alpha + \frac{\alpha_t}{\sigma_\theta}\right)\boldsymbol{\nabla}k_\theta\right] + P_\theta - C_\mu\, k_\theta\, e^{\Omega_\theta}\,, \tag{33}$$

$$\begin{aligned}\frac{\partial \Omega_\theta}{\partial t} + \mathbf{u}\cdot\boldsymbol{\nabla}\Omega_\theta = {}& \boldsymbol{\nabla}\cdot\left[\left(\alpha + \frac{\alpha_t}{\sigma_{\varepsilon_\theta}}\right)\boldsymbol{\nabla}\Omega_\theta\right] + \frac{2}{k_\theta}\left(\alpha + \frac{\alpha_t}{\sigma_{\varepsilon_\theta}}\right)\boldsymbol{\nabla}k_\theta\cdot\boldsymbol{\nabla}\Omega_\theta + \\ & + \left(\alpha + \frac{\alpha_t}{\sigma_{\varepsilon_\theta}}\right)\boldsymbol{\nabla}\Omega_\theta\cdot\boldsymbol{\nabla}\Omega_\theta + \frac{c_{p1}-1}{k_\theta}P_\theta + \frac{c_{p2}}{k}P_k - \left(c_{d1}-1\right)e^{\Omega_\theta} - c_{d2}C_\mu e^{\Omega}\,.\end{aligned} \tag{34}$$

The eddy viscosity ν_t and the eddy thermal diffusivity α_t are modeled as

$$\nu_t = C_\mu k \tau_{lu}\,, \qquad \alpha_t = C_\theta k \tau_{l\theta}\,. \tag{35}$$

For the modeling of the characteristic time scales for dynamic and thermal turbulence one can see [7, 8, 9]. With this turbulence model one can correctly reproduce the near wall behavior of the turbulence variables, which means $k \propto \delta^2$, $\nu_t \propto \delta^3$, $k_\theta \propto \delta^2$ assuming zero temperature fluctuations, and $\alpha_t \propto \delta^3$.

3 Numerical results

In this section we present the results obtained from the simulations of fully developed turbulent flows of liquid metals in several geometries. The plane channel and cylindrical duct geometries are investigated for different values of Reynolds numbers. A complex 19-pin hexagonal

rod bundle is simulated for a specific pitch-to-diameter ratio and Reynolds number. In Table 3 the values of the physical properties are reported. In particular those values are representative of Lead-Bismuth-Eutectic (LBE) which has a molecular Prandtl number $Pr = 0.025$.

We implement the system (31-34) and the Navier-Stokes equations in an in-house finite element code. We employ Taylor-Hood finite elements for the system of Navier-Stokes in order to satisfy the inf-sup condition and this system is solved with a standard projection method. The two systems of turbulence equations are solved with standard quadratic finite elements.

3.1 Plane channel

The plane channel is one of the simplest type of geometry that can be simulated and many Direct Numerical Simulation are available for this kind of flow. In particular for fully developed turbulent flows results of the dynamical turbulence for the cases of friction Reynolds number $Re_\tau = 180$, 395, 640, 950, 2000 and 4200 are available [13, 14, 15], while results of fully developed thermal turbulent flow for a fluid with $Pr = 0.025$ are available only for the cases of friction Reynolds number $Re_\tau = 180$, 395 and 640 [13]. The domain consists of two plates located at a distance $L = 0.0605$ m, with infinite dimensions in the other directions. On the wall a uniform heat flux of 3.6×10^5 W/m^2 is applied. The condition of fully developed turbulent flow is imposed with periodic boundary conditions on the inlet and outlet of the channel.

We simulate seven test cases with Reynolds number $Re \simeq 5700$ (A), 14000 (B), 24000 (C), 37000 (D), 86000 (E), 198000 (F) and 325000 (G). They correspond to friction Reynolds numbers $Re_\tau \simeq 180$, 395, 640, 950, 2000, 4200 and 6600. All simulations are performed using a spatial discretization of the physical domain in order to have the first mesh point at $y^+ < 1$.

Property	Symbol	Value	Unit
Viscosity	μ	0.00184	Pa s
Density	ρ	10340	Kg/m^3
Thermal conductivity	λ	10.72	W/(m K)
Heat specific capacity	C_p	145.75	J/(Kg K)

Table 3: Physical parameters used in the CFD simulations.

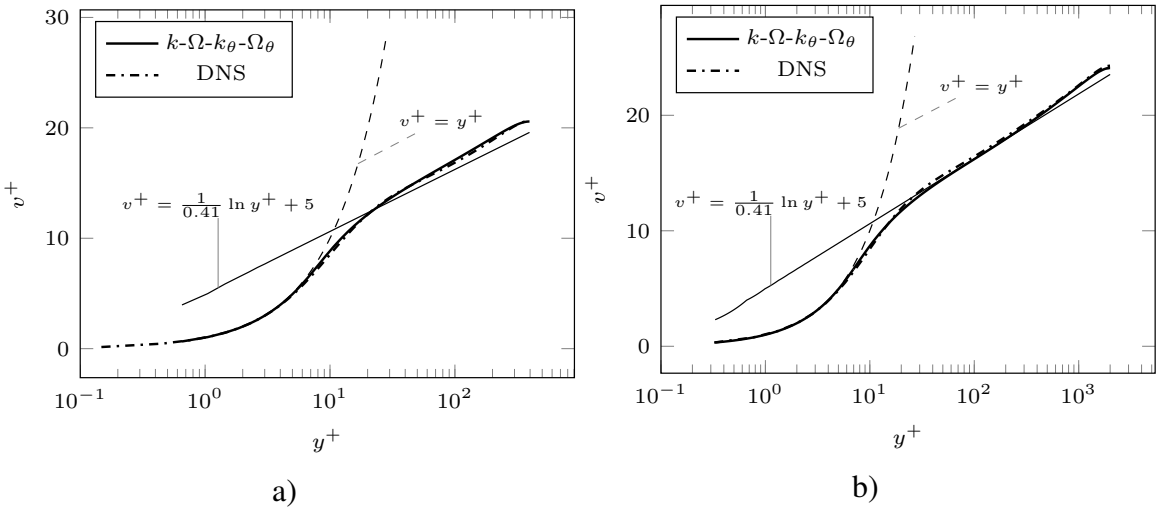

Figure 1: Non dimensional velocity profiles as a function of the non dimensional distance from the wall y^+. Cases $Re_\tau = 395$ (a) and $Re_\tau = 2000$ (b) obtained with the k-Ω turbulence model (continuous) and from DNS simulation data (dash-dotted).

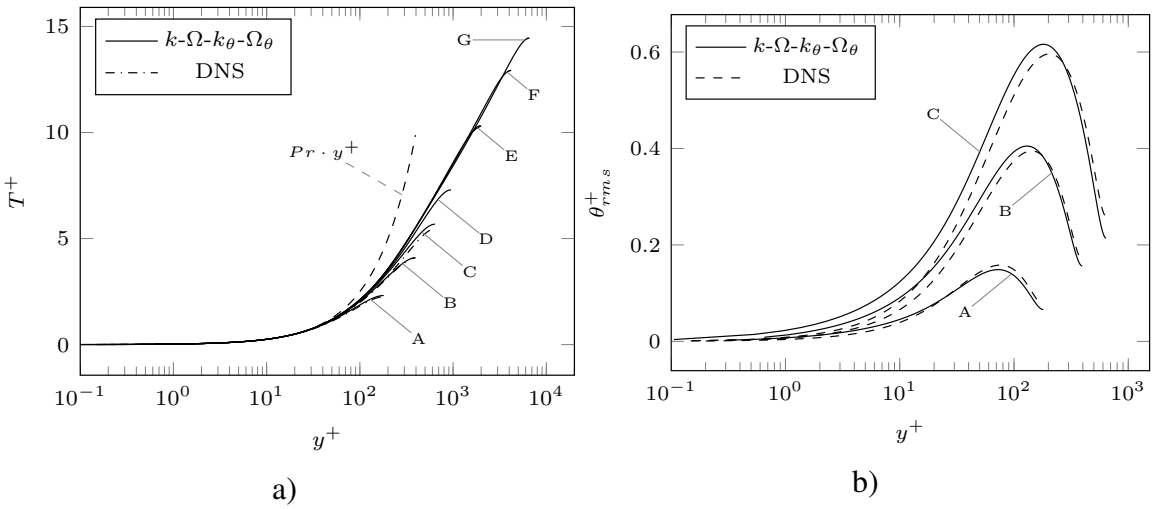

Figure 2: Profile of the non dimensional temperature T^+ (a) and of the root mean squared temperature fluctuations θ_{rms} (b) as a function of the non dimensional distance from the wall y^+. DNS results are reported for the cases $Re_\tau = 180$, 395 and 640 (dash-dotted).

In Figure 1 a comparison is shown between the results obtained with the k-Ω turbulence model and those obtained with DNS for the cases of $Re_\tau = 395$ and $Re_\tau = 2000$. In this Figure the velocity v has been non dimensionalized with the friction velocity v_τ which is calculated as $v_\tau = \sqrt{\tau_w/\rho}$, where τ_w is the wall shear stress, and plotted against the non dimensional wall distance $y^+ = yv_\tau/\nu$. The linear behavior $v^+ = y^+$ and the logarithmic one $v^+ = 1/0.41\ln(y^+) + 5$ are well reproduced in both cases.

The profiles of the non dimensional temperature are shown in Figure 2 (a), together with the results of DNS simulations for the cases where they are available. The temperature has been non dimensionalized with the friction temperature T_τ defined as $T_\tau = q/(v_\tau \rho C_p)$, where q is the heat flux applied on the wall. The linear behavior $T^+ = Pr\, y^+$ is well reproduced for every single case. In Figure 2 (b) the values of root mean squared temperature fluctuations $\theta_{rms} = \sqrt{2k_\theta}$ are compared with the ones obtained with DNS simulations. We can see that there is a good agreement between the results of the turbulence model and Direct Numerical Simulation data.

3.2 Cylindrical pipe

For the cylindrical pipe the DNS data for the dynamical turbulence are available for the cases $Re_\tau = 180$, 360, 550, and 1000 [16]. The results are thus validated using the experimental correlations for the Nusselt number. In particular we refer to the Kirillov correlation as the main reference for the cylindrical geometry [17]. This correlation is claimed to be valid for $10^4 < Re < 5 \cdot 10^6$. The Nusselt number is calculated as a function of the Peclet number $Pe = Pr \cdot Re$

$$Nu = 4.5 + 0.018\, Pe^{0.8}\,. \tag{36}$$

For the cylindrical case we simulate fully developed turbulent flows with $Re_\tau = 180$ (A), 360 (B), 550 (C), 1000 (D), 3580 (E), 5840 (F) and 6860 (G). The corresponding values of the Reynolds number for these cases are 5760, 12770, 20700, 41000, 165000, 286000 and 341000. As in the plane channel case, all the simulations for the cylindrical pipe are performed refining the mesh in order to have the first mesh point with $y^+ < 1$. In Figure 3 (a) the profiles of the non dimensional temperature T^+ are shown as functions of the non dimensional distance

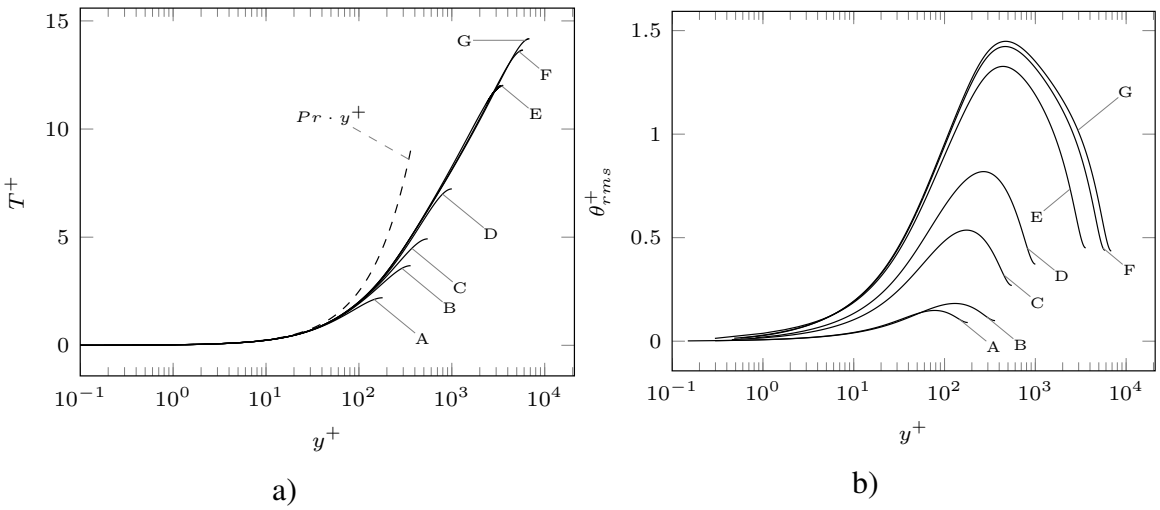

Figure 3: Non dimensional profiles of: mean temperature (a) and root mean squared values of temperature fluctuations (b) as functions of the non dimensional distance from the wall y^+ for all the simulated cases.

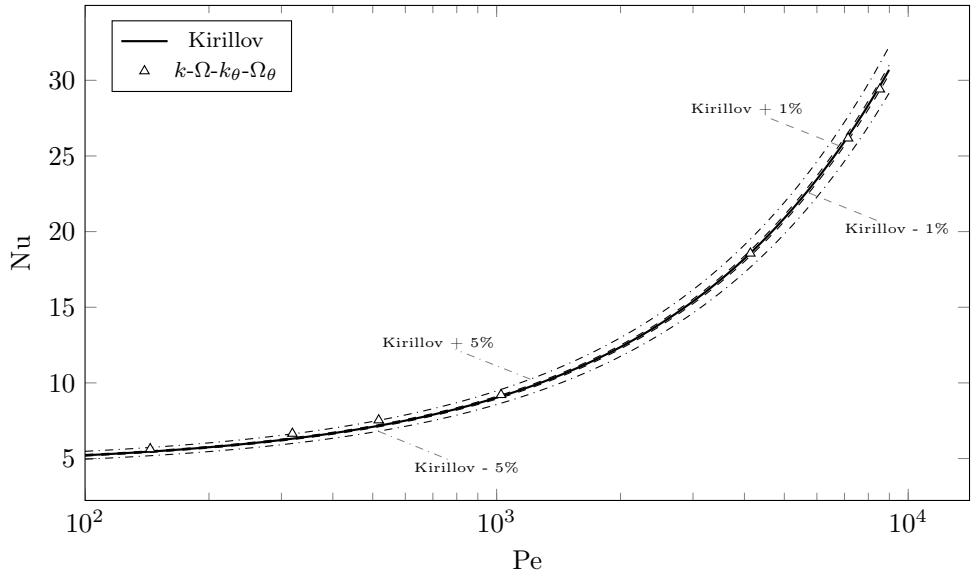

Figure 4: Comparison between the Kirillov correlation for the Nusselt number and the values of Nu calculated with the four parameters turbulence model.

from the wall y^+. In every case the linear behavior $T^+ = Pr\, y^+$ is well reproduced, as can be seen from the comparison with the dashed line. In Figure 3 (b) the non dimensional root mean squared values of temperature fluctuations $\theta^+_{rms} = \sqrt{2k_\theta}/T_\tau$ are presented for all the simulated cases.

Finally we calculate the Nusselt number values and compare them with the Kirillov correlation. This comparison is presented in Figure 4 where the values of the Nusselt number are plotted against the Peclet number. As it can be seen some differences between the correlation data and the values calculated with the turbulence model appear in the low velocity region (Pe $< 10^3$). The differences with the Kirillov correlation, in this region, are included within 5%. In the high velocity region with Pe $> 10^3$ our values are closer to the Kirillov correlation. As shown in the Figure the values are included within 1%.

3.3 Hexagonal rod bundle

Property	Symbol	Value	Unit
Number of pins	n	19	-
Pin diameter	d	0.0082	m
Pitch to diameter ratio	p/d	1.3	-
Height	z	2	m
Minimum pin-wall distance	l	0.00172	m
Hydraulic diameter	D_h	7.706×10^{-3}	m

Table 4: Geometrical parameters of the simulated hexagonal bundle.

In this Section we present the results of a simulation of a 19-pins hexagonal rod bundle. In Figures 5 (a) and (b) a geometrical representation of the whole bundle is given. The bundle is bounded by adiabatic solid walls. This particular configuration is used for experimental analysis [18]. Due to the symmetry of the geometry and boundary conditions it is possible to simulate only one twelfth of the entire bundle.

A transverse section of the computational domain can be seen in Figures 6-7 while the geometrical parameters of the bundle are reported in Table 4. In the simulated case the velocity and the dynamical turbulence are fully developed, so we impose periodic boundary conditions at the inlet and outlet of the bundle. On the wall boundaries we set

$$u = v = 0\,, \quad \frac{\partial w}{\partial n} = \frac{\mu}{\delta}\,, \quad \frac{\partial k}{\partial n} = 2\frac{k}{\delta}\,, \quad \Omega = \ln\left(\frac{2\nu}{C_\mu \delta^2}\right), \tag{37}$$

where n indicates the direction normal to the wall and δ the wall distance. On the other boundaries we impose a symmetry condition. For the thermal field we impose a fixed uniform temperature of 573 K at the inlet of the bundle, so k_θ is set to zero and Ω_θ is set to the same value that it has on the wall boundaries. On the pin walls we impose a uniform heat flux of 3600 W/m^2, while the external wall is considered adiabatic, $\partial T/\partial n = 0$. For the thermal turbulent variables

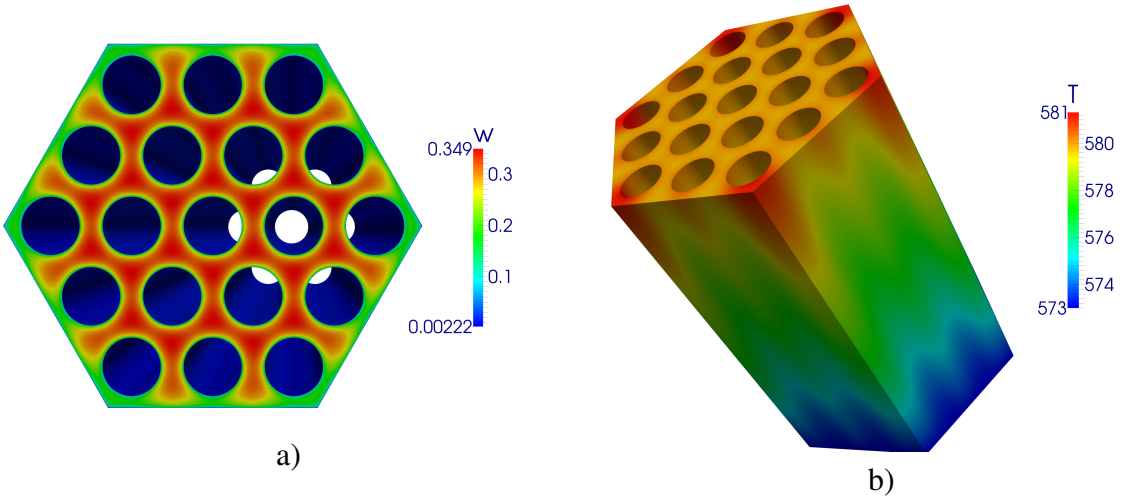

a) b)

Figure 5: Front view of the hexagonal bundle with the velocity field (a) and a scaled view of the whole hexagonal bundle with the thermal field (b).

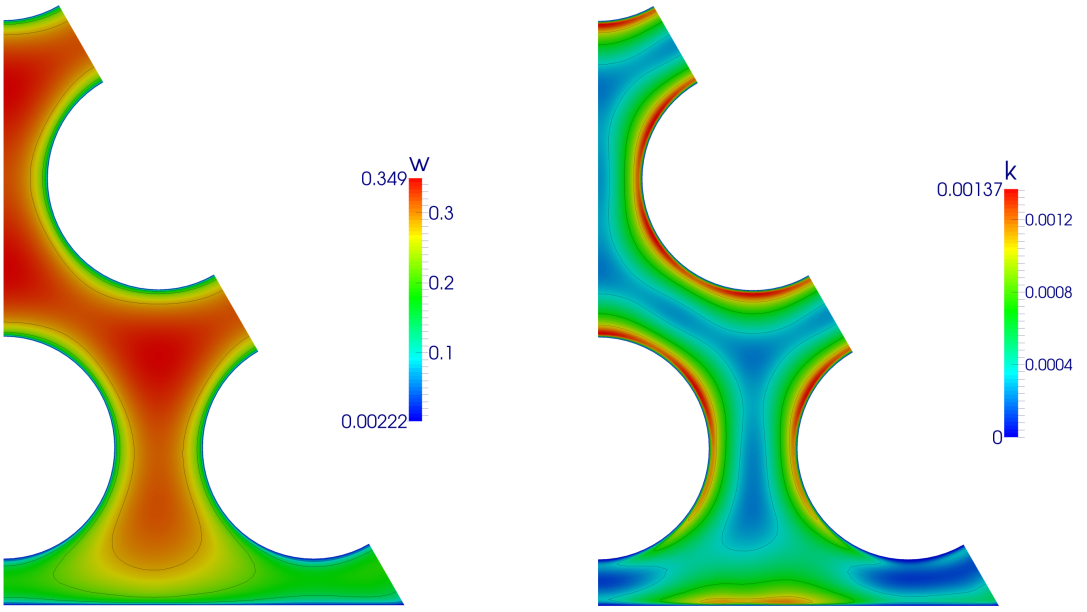

a) b)

Figure 6: Distribution of the axial component w of the velocity field (a) and of the turbulent kinetic energy k (b) on a transverse section of the bundle.

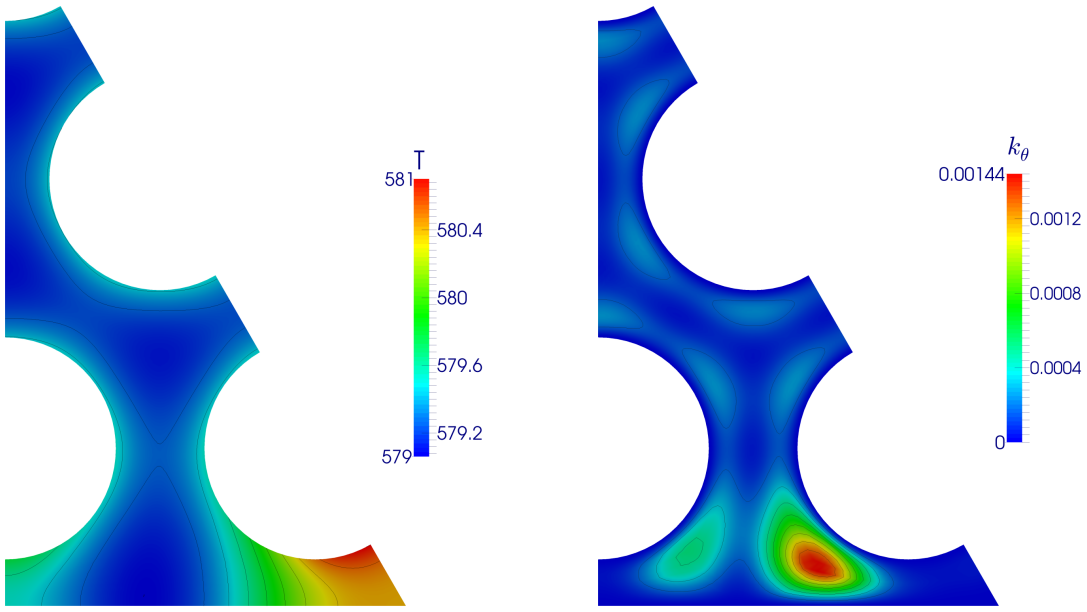

a) b)

Figure 7: Distribution of the temperature T field (a) and of the mean squared temperature fluctuations k_θ (b) on a transverse section of the bundle.

on every wall we impose the following boundary conditions

$$\frac{\partial k_\theta}{n} = 2\frac{k_\theta}{\delta}\,, \quad \Omega_\theta = \ln\left(\frac{2\alpha}{C_\mu \delta^2}\right). \tag{38}$$

At the outlet of the bundle we consider that no heat exchange occurs, so we impose a null derivative in the direction normal to the outlet surface for T and for k_θ and Ω_θ. The physical properties of the fluid are the same shown in Table 3. The mean axial velocity is $w_{mean} = 0.23$

m/s, so the Reynolds number is $Re = 10070$.

In Figure 5 (a) the axial component of the velocity field is shown at the bundle outlet while in Figure 5 (b) the temperature field is presented in a scaled view of the whole bundle. In Figure 6 (a) the axial velocity is reported on a transverse section of the bundle. In the region near the adiabatic wall the velocity is smaller than in the remaining part of the domain. Due to this phenomenon we have some areas characterized by a low turbulence in the same region, as it can be seen from Figure 6 (b), where the field of turbulent kinetic energy is shown. We recall that we simulate the condition of fully developed turbulent flow, so the distributions shown in Figure 6 (a) and in Figure 6 (b) are the same for every transverse section along the axial coordinate z.

The temperature distribution for the transverse section at $z = 1.8$ m is shown in Figure 7 (a). As we can see the temperature distribution is almost uniform except in the region near the adiabatic wall where a stagnation point appears. In particular the temperature distribution reaches its maximum value in the corner region, as it can be better seen from Figure 5 (b). In the region near the adiabatic wall the temperature changes sharply. This fact reflects the distribution of the mean squared value of the temperature fluctuations, which is reported in Figure 7 (b). The transverse section is at the same height as Figure 7 (a).

4 Conclusion

In this work we have proposed a new four parameter turbulence model with logarithmic variables. The model has been tested in simulations of fully developed turbulent flows of low Prandtl number fluids ($Pr = 0.025$) and compared with reference results available in literature. For the case of plane channel, where more DNS data are available for both dynamical and thermal turbulence, the results of the new four parameter turbulence model show a good agreement with DNS results. For the case of cylindrical pipe we focused our attention on the values of the Nusselt number obtained for all the simulated cases because a few DNS data for the thermal field are available in literature. The obtained results are very close to the Kirillov correlation, which has been taken as the main reference for the Nusselt number prediction. Finally some preliminary results of the application of the turbulence model on a complex three-dimensional geometry have been reported, showing the robustness of the model also in thermally developing three-dimensional flows. The new turbulence model can thus be used as a reliable tool for the study of turbulent flows characterized by low Prandtl numbers.

REFERENCES

[1] X. Cheng and N. Tak, *Investigation on turbulent heat transfer to lead-bismuth eutectic flows in circular tubes for nuclear applications*, Nuclear Engineering and Design, Vol.236, pp. 385-393, 2006.

[2] X. Cheng and N.I. Tak, *CFD analysis of thermal-hydraulic behavior of heavy liquid metals in sub-channels*, Nuclear Engineering and Design, Vol. 236, pp. 1874-1885, 2006.

[3] Y. Nagano and M. Shimada, *Development of a two equation heat transfer model based on direct simulations of turbulent flows with different Prandtl numbers*, Physics of Fluids, Vol. 8, pp. 3379-3402, 1996.

[4] K. Abe, T. Kondoh and Y. Nagano, *A new turbulence model for predicting fluid flow and heat transfer in separating and reattaching flows II. Thermal field calculations*, International Journal of Heat Mass Transfer, Vol. 38 (8), pp. 1467-1481, 1995.

[5] B. E. Launder, G. J. Reece and W. Rodi, *Progress in the development of a Reynolds-stress turbulence closure*, Journal of Fluid Mechanics, Vol. 37 (3), pp. 537-566, 1975.

[6] D. Cerroni, R. Da Vià, S. Manservisi, F. Menghini, G. Pozzetti and R. Scardovelli, *Numerical validation of a k-ω-k_θ-ω_θ heat transfer turbulence model for heavy liquid metals*, Journal of Physics: Conference Series, Vol. 655, 012046, 2015.

[7] S. Manservisi and F. Menghini, *A CFD Four Parameter Heat Transfer Turbulence Model for Engineering Applications in Heavy Liquid Metals in rod bundle geometries*, International Journal of Heat and Mass Transfer, Vol. 69, pp. 312-326, 2014.

[8] S. Manservisi and F. Menghini, *Triangular rod bundle simulations of a CFD k-ϵ-k_θ-ϵ_θ Heat Transfer Turbulence Model for Heavy Liquid Metals*, Nuclear Engineering and Design, Vol. 273, pp. 251-270, 2014.

[9] S. Manservisi and F. Menghini, *CFD simulations in heavy liquid metal flows for square lattice bare rod bundle geometries with a four parameter heat transfer turbulence model*, Nuclear Engineering and Design, Vol. 295, pp. 251-260, 2015.

[10] K. Abe, T. Kondoh and Y. Nagano, *A two-equation heat transfer model reflecting second-moment closures for wall and free turbulent flows*, International Journal of Heat and Fluid Flow, Vol. 17, pp. 228-237, 1996.

[11] H. Hattori, Y. Nagano and M. Tagawa, *Analysis of turbulent heat transfer under various thermal conditions with two-equation models*, Engineering Turbulence Modeling and Experiments 2 (Edited by W. Rodi and F. Martelli), pp. 43-52, 1993.

[12] F. Ilinca, J. F. Hetu, and D. Pelletier, *A unified finite element algorithm for two-equation models of turbulence*, Computers & Fluids, Vol. 27 (3), pp. 291-310, 1998.

[13] H Kawamura, H Abe and Y Matsuo, *DNS of turbulent heat transfer in channel flow with respect to Reynolds and Prandtl number effects.*, International Journal of Heat and Fluid Flow, Vol. 20, pp. 196-207, 1999.

[14] S. Hoyas and J. Jiménez, *Reynolds number effects on the reynolds-stress budgets in turbulent channels*, Physics of Fluids, Vol. 20 (10), 101511, 2008.

[15] A. Lozano-Durn and J. Jiménez, *Effect of the computational domain on direct simulations of turbulent channels up to re_τ = 4200*, Physics of Fluids, Vol. 26 (1), 011702, 2014.

[16] G.K. El Khoury, P. Schlatter, A. Noorani, P.F. Fischer, G. Brethouwer and A.V. Johansson, *Direct numerical simulation of turbulent pipe flow at moderately high Reynolds numbers*, Flow, Turbulence and Combustion, Vol. 91 (3), pp. 475-495, 2013.

[17] P. Kirillov and P.A. Ushakov, *Heat transfer to liquid metals: specific features, methods of investigation, and main relationships*, Thermal Engineering, Vol. 48 (1), pp. 50-59, 2001.

[18] J. Pacio, K. Litfin, A. Batta, M. Viellieber, A. Class, H. Doolaard, F. Roelofs, S. Manservisi, F. Menghini and M. Böttcher, *Heat transfer to liquid metals in a hexagonal rod bundle with grid spacers: Experimental and simulation results*, Nuclear Engineering and Design, Vol. 290, pp. 27-39, 2014.